The Astrophysical Journal, 617:551–558, 2004 December 10

THE ZEEMAN-SENSITIVE EMISSION LINES OF Mg I AT 12 MICRONS IN PROCYON

N. Ryde[1,2] and A. J. Korn
Department of Astronomy and Space Physics, Uppsala University, Box 515, SE-75120 Uppsala, Sweden;
ryde@astro.uu.se, akorn@astro.uu.se

M. J. Richter[2]
Department of Physics, University of California, Davis, CA 95616;
richter@physics.ucdavis.edu

and

F. Ryde[3]
Stockholm Observatory, AlbaNova University Center, SE-10691 Stockholm, Sweden;
felix@astro.su.se
Received 2004 July 2; accepted 2004 August 20

ABSTRACT

Emission lines of magnesium at 12 μm have been observed in the spectrum of Procyon. We reproduce the observed disk-averaged line flux from Procyon (as well as the observed intensity profiles from the Sun) by calculating the line formation and relaxing the assumption of local thermodynamic equilibrium. We find that the lines in Procyon are formed in the photosphere in the same manner as the solar lines. We discuss our modeling of these Rydberg lines and evaluate, among other things, the importance of the ionizing flux and updated model-atom parameters. The lines are of large diagnostic value for measurements of stellar magnetic fields through their Zeeman splitting. We have not, however, detected splitting of the Mg I lines in Procyon. Using simple arguments, we believe that we would have detected a magnetic field had it been of a strength larger than approximately 800 G covering more than a quarter of the surface. We discuss the prospects for future use of the Zeeman-sensitive, mid-infrared Mg I emission lines as a diagnostic tool for stellar magnetic fields.

Subject headings: infrared: stars — stars: atmospheres — stars: individual (α Canis Minoris) — stars: magnetic fields

1. INTRODUCTION

Although magnetic fields affect, and sometimes dominate, the appearance of cool stars, direct detection and determination of magnetic field strengths are difficult. Methods involving polarized light and magnetograms are problematic for cool stars with assumed solar-like magnetic geometries (Saar 1988). On the other hand, studies of unpolarized Zeeman splitting in the near-infrared (NIR) have given a large scientific return (see, e.g., Muglach & Solanki 1992; Solanki et al. 1992; Solanki 1994; Valenti et al. 1995; Johns-Krull et al. 1999).

Mg I emission lines at 12 μm in sunspot penumbrae and plages clearly show Zeeman splitting and so trace the local magnetic field (see, e.g., Brault & Noyes 1983; Bruls & Solanki 1995; Bruls et al. 1995). Zeeman splitting is independent of the field direction and will show up even in a disk-averaged spectrum from a star with a disorganized field structure, which is not the case for polarized light. The wavelength dependence of Zeeman broadening compared to other types of broadening results in the 12 μm lines being more Zeeman-sensitive than NIR lines. Furthermore, the 12 μm lines probe other atmospheric layers than do the NIR lines. Thus, these lines potentially offer an excellent method for measuring stellar disk-averaged magnetic fields.

Solar emission features at 12 μm were first mentioned by Murcray et al. (1981) and attracted much attention during the 1980s. Chang & Noyes (1983) identified the two strongest emission lines as coming from transitions between Rydberg states in Mg I. Lemke & Holweger (1987) showed that the emission could be formed in the photosphere through stimulated emission and different departures from local thermodynamic equilibrium (LTE) for the lower and upper levels. The first non-LTE modeling giving the lines in emission was by Carlsson et al. (1990, 1992b) and Chang et al. (1991). The line formation process was first explained successfully and in detail by Carlsson et al. (1992b). They concluded that the lines were photospheric in origin and accounted very well for their emission strengths and complicated intensity profiles as a function of the viewing angle on the solar disk. Uitenbroek & Noyes (1996), observing just one of the two lines, detected emission from the K giant α Boo and saw absorption from the five M giants and supergiants in their sample. Their model calculations were unable to fit the data. Ryde & Richter (2004) detected and analyzed both Mg I emission lines from Procyon (α CMi) observed at a resolving power of $R = 86,000$. As high-resolution, mid-infrared spectrographs become available on 8–10 m telescopes, these lines will be observed in many more stars. A first step toward the sophisticated use of these lines for measuring stellar magnetic fields is the understanding of their formation and response to a broad range of stellar parameters.

[1] Postdoctoral Fellow in 2001–2002 at the Department of Astronomy, University of Texas, Austin, TX 78712.

[2] Visiting Astronomer at the Infrared Telescope Facility, which is operated by the University of Hawaii under cooperative agreement NCC 5-538 with the National Aeronautics and Space Administration, Office of Space Science, Planetary Astronomy Program.

[3] Postdoctoral Fellow in 2001–2002 at the Department of Physics, Stanford University, Stanford, CA 94305.

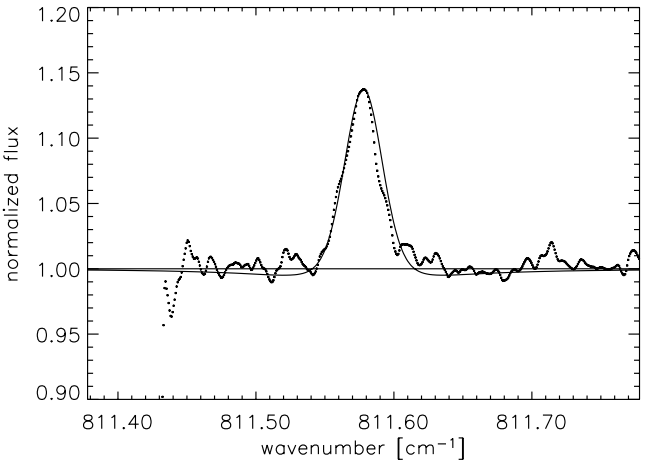

FIG. 1.—Mg I emission line at 12.32 μm (*dotted line*) observed from Procyon. The solid line shows the model emission line, and a horizontal line showing the normalization level is added.

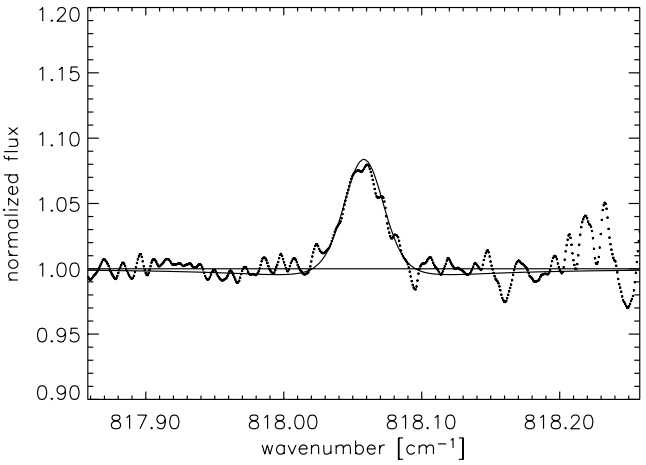

FIG. 2.—Mg I line at 12.22 μm (*dotted line*) observed from Procyon. As in Fig. 1, the model is shown by a solid line, and the normalization level is shown by a horizontal line.

In this paper, we discuss our analysis of the magnesium emission lines detected from Procyon. We discuss the atomic model of Mg I and the assumptions made in our non-LTE calculation, such as the collisional rates, the atmospheric radiation field used, and the validity of the assumption of atmospheric homogeneity. We conclude with a discussion on using these lines for determining disk-averaged magnetic field strengths in stars and an estimate of the maximum field strength and corresponding filling factor allowed by our observations.

2. OBSERVATIONS

We observed Procyon with the Texas Echelon-Cross-Echelle Spectrograph (TEXES; Lacy et al. 2002), a visitor instrument at the NASA 3.0 m Infrared Telescope Facility (IRTF) on Mauna Kea in Hawaii. The observations took place over a number of observing runs from 2000 November through 2004 January. We used the high-resolution, cross-dispersed mode, with orders covering $\sim$0.67 cm^{-1} and a total spectral coverage of roughly 0.6% ($\sim$5 cm^{-1}). Separate settings were required for each Mg I line. Observations of narrow-line sources indicate that the instrumental line profile has a Gaussian core with a FWHM of 3.5 km s^{-1}, i.e., $R \sim 86{,}000$, and wings that are only slightly stronger than a Gaussian distribution.

Our observations consisted of calibration frames mixed with nodded observations of Procyon. Before each data file, we observed an ambient temperature blackbody, a low-emissivity surface, and the sky, as described in Lacy et al. (2002). The blackbody serves as a flat field and provides first-order sky correction after subtracting the sky emission frame. We integrated for approximately 1 s frame^{-1} to overcome detector readout noise. Depending on conditions, we summed 6–8 frames before moving the telescope by 4″–5″, thus placing Procyon at a different position along the slit and creating a nod pair. After roughly 10 minutes of integrating on target, we started another series with the calibration frame.

We used the standard TEXES data reduction pipeline (Lacy et al. 2002) to reduce the data. We fixed spikes and cosmic-ray hits using the time series, rectified the echellegram so that the spatial and dispersion axes run along rows and columns of the detector, and removed the sky and telescope background by differencing each nod pair. The individual nod pairs were combined after allowing for as much as a 1″ shift along the slit and after weighting the pairs according to the square of an estimated signal-to-noise ratio. Extraction of the final spectrum for a given data set used the spatial profile derived from the data, with a mean set to zero, as the extraction template. To set the frequency scale, we used the location and frequency of telluric atmospheric lines, which typically give an accuracy better than 1 km s^{-1}.

After reducing a given data set, we normalized the continuum using a sixth-order Legendre polynomial and then combined appropriate data files. Procyon has almost no photospheric features at this wavelength, so determining the continuum is straightforward and reliable. The telluric atmosphere at the Mg I wavelengths is very clean, so we did not need to correct for telluric features. Slight variations in wavelength setting from night to night resulted in increased noise where fewer data could be co-added.

In the observations presented in Figures 1 and 2, the signal-to-noise ratio is found to be 130 : 1 and 100 : 1, respectively.

3. MODELING

In Ryde & Richter (2004) we presented the detection of the 12 μm Mg I emission from Procyon and briefly described our modeling of the emission. Here we describe the modeling in more detail.

We analyze the line formation and the spectral synthesis of the emission lines with a full non-LTE calculation using the code MULTI (Carlsson 1986). We have used the model atom of Carlsson et al. (1992b), which was slightly improved by Bruls et al. (1995) and kindly provided by M. Carlsson. To test our application of the model, we first reproduced the excellent fits of the intensity profiles measured at different locations on the solar disk, as presented in Carlsson et al. (1992b). Our model atom is identical to the one used by Bruls et al. (1995), except that, in order to fit the solar lines with our modeling, we have increased the collisional cross sections for the two 12 μm lines by 50%, as discussed in § 4.4. In Figures 3 and 4 we show the observed intensity profiles of the solar Mg I lines (Brault & Noyes 1983) measured at $\mu = \cos\theta = 0.2$, 0.5, and 1.0 on the solar disk. Our best model is shown by the solid lines.

The model magnesium atom consists of 66 levels and includes 315 line transitions and 65 bound-free transitions from all levels. The Mg II ground state is included. We solve the equations of statistical equilibrium governing the level populations for all levels. A photospheric radiation field is included for

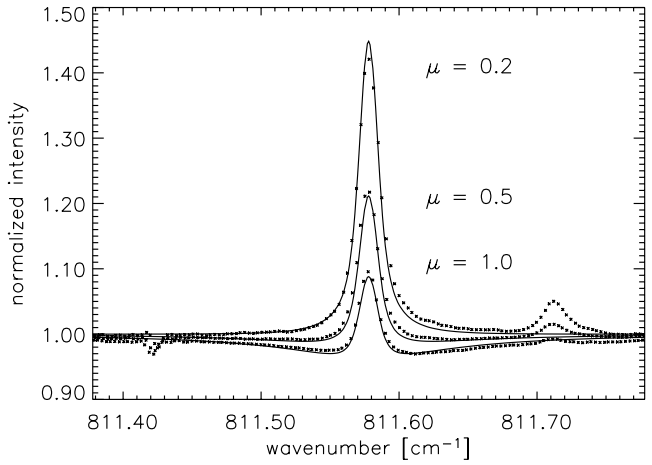

FIG. 3.—Measured solar intensity profiles of the Mg I line at 12.32 μm (*dotted lines*) observed by Brault & Noyes (1983). Three positions on the solar disk are shown, with $\mu = \cos\Theta$ giving the position on the disk. The solid lines show our modeled emission lines. The small emission line at 811.71 cm^{-1} is due to silicon, and the absorption at 811.42 cm^{-1} is a telluric absorption line.

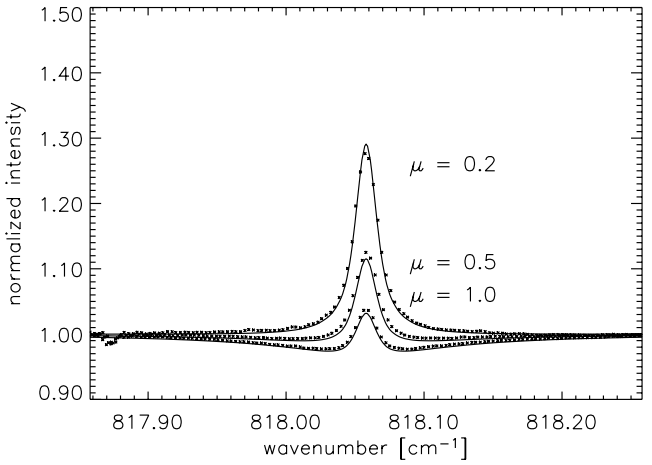

FIG. 4.—Brault & Noyes (1983) observations of the 12.22 μm Mg I line (*dotted lines*) observed from the Sun. As in Fig. 3, the model is shown by solid lines. The absorption feature at the far left is a telluric absorption line.

calculating the photoionization rates by incorporating the calculated specific mean intensity field for all depths from a model atmosphere. This allows full line blanketing to be considered, especially in the ultraviolet wavelength region that affects mainly photoionization from the lowest states.

The physical structure of the atmosphere is modeled with a one-dimensional, hydrostatic, flux-conserved, nonmagnetic, LTE model atmosphere, calculated using frequency opacity sampling (OS) with the MARCS code. MARCS was first developed by Gustafsson et al. (1975) and has been successively updated ever since (B. Gustafsson et al. 2004, in preparation). Data on absorption by atomic species come from the VALD database (Piskunov et al. 1995) and R. L. Kurucz (1995, private communication). Absorption by molecules is included but not very important for Procyon. The model atmosphere has a plane-parallel geometry and is horizontally homogeneous, with 55 depth points extending out to an optical depth, calculated in the continuum at 500 nm, of $\log \tau_{500} \sim -5$. No chromosphere is included. Our calculation provides the self-consistent, specific, mean intensity field for all depths mentioned above.

The fundamental stellar parameters of Procyon, used in the calculation of the model atmosphere, are based on the discussion in Allende Prieto et al. (2002): $T_{\rm eff} = 6512 \pm 50$ K, $\log g = 3.96 \pm 0.02$ cgs, $M = 1.42 \pm 0.06\ M_{\odot}$, $R = 2.07 \pm 0.02\ R_{\odot}$, and a metallicity (iron abundance) slightly lower than solar. Fuhrmann (1998) measures a slightly supersolar Mg abundance in LTE, whereas Korn (2002) measures a slightly subsolar Mg abundance in a non-LTE analysis. In the following discussion we assume a solar abundance mixture as given by Grevesse & Sauval (1998).

The 12 μm emission-line parameters are given in Table 1. To fit the width of the lines in Procyon, we need to convolve our synthetic lines with a Gaussian distribution having a FWHM of 9.5 km s^{-1}. This includes the atmospheric macroturbulence, the projected rotation of the star, and the contribution of the instrumental profile and is somewhat larger than the value Gray (1981) found for Procyon from optical spectra.

4. ANALYSIS

The results of our model for the Mg I lines $3s7i^{1,3}I^e \rightarrow 3s6h^{1,3}H^o$ (811.578 cm^{-1}) and $3s7h^{1,3}H^o \rightarrow 3s6g^{1,3}G^e$ (818.058 cm^{-1}), in Procyon are shown in Figures 1 and 2, respectively. The model fits agree well with the observations. It is interesting to note that the Mg I emission in Procyon is of the same magnitude as that from the Sun. As explained in Ryde & Richter (2004), although the higher temperatures in the atmosphere of Procyon ionize a factor of 10 more magnesium atoms, neutral magnesium is more highly excited. This compensates for the lower number of atoms and gives rise to a similar number of effective emitters/absorbers.

In Figure 5, we have plotted the departures from Boltzmann level populations yielded by our non-LTE calculations, both for Procyon and for the Sun, as a function of optical depth. We show only the levels involved in the formation of the Mg I emission lines and the ground states of Mg I and Mg II. The departure coefficients are very similar for both stars, indicating that the same formation process is at work. In addition, they are quite similar for both the upper and lower states; the departure coefficient of the upper level is of the order of 10% larger than that of the lower state outside of $\log \tau_{500} \sim -2.5$. Thus, the lower levels depart more from LTE. Whereas for the Sun the population of Mg II is slightly larger than that of LTE, for Procyon the Mg II population is very close to that of LTE. In Figure 5, the departure coefficient of Mg II in Procyon is enlarged.

The small difference between the level departures generating the lines has a large impact on the emergent line strengths and is the direct cause of the observed emission. As also explained in detail in Carlsson et al. (1992b), the main cause of the emission is the divergence of the departure coefficients of the two levels, which starts to be pronounced at a depth of $\log \tau_{500} \sim -2$ and increases outward through the atmosphere. Although small, the divergence causes the line source function to grow rapidly outward in the atmosphere, a fact that increases with wavelength (because of the increasing influence of stimulated emission).[4] The rapid outward growth of the source function results in the emission lines. To a lesser degree, the line opacity is also affected by the departures.

The departure coefficients of the upper and lower states, respectively, of the two Mg I emission lines follow each other exactly, since they have the same n quantum numbers. The

[4] In passing, however, it can be noted that the emission is not caused by truly inverted populations, as is the case in a laser.

TABLE 1
LINE DATA OF THE 12 μm LINES

Wavelength λ (Å)	Wavenumber σ (cm^{-1})	Transition	E_{up} (eV)	E_{low} (eV)	log gf (Green et al. 1957) (cgs)	Landé Factor g (Lemoine et al. 1988)
12.3217.....	811.578	$3s7i^{1,3}I^e - 3s6h^{1,3}H^o$	7.3693	7.2686	1.95	0.99 ± 0.01
12.2241.....	818.058	$3s7h^{1,3}H^o - 3s6g^{1,3}G^e$	7.3691	7.2676	1.73	1.00 ± 0.01

reason for this is our inclusion of, following Carlsson et al. (1992b), "quasi-elastic *l*-changing"[5] collisions with neutral particles, which keep all close-lying Rydberg states with common principal quantum numbers, *n*, in relative thermalization.

The average height of formation of the continuum lies at approximately $\log \tau_{500} = -1.6$, where H^-_{ff} dominates as the continuous opacity source. The average height of formation of the line center, calculated in non-LTE, lies at $\log \tau_{500} \sim -2.7$, but the lines have contribution functions extending over approximately $-4 < \log \tau_{500} < -1$. The monochromatic source function at the wavelengths of the line center decouples from the thermalized Planck function around $\log \tau_{500} \sim -1.5$. The line profile probes the minimum of the source function that causes the troughs of the wings of the observed line profiles. These are especially prominent in the intensity profiles in the Sun; see Figures 3 and 4. The troughs are also present in our modeled line profiles of the flux from Procyon, but they are too shallow to be verified in the observed profiles (see Figs. 1 and 2).

The observed emission lines are formed as a result of a non-LTE flow cycle ("photon suction"; see Carlsson et al.). The process is driven by lines originating from levels of high-excitation energy ($\chi_{exc} \sim 7$ eV) that become optically thin in the photosphere. This leads to overpopulated levels at $\chi_{exc} \sim 6$ eV that are subsequently photoionized directly or through a state at ~3 eV. Note that in the case of the Sun, more than 93% of the magnesium is singly ionized, while in Procyon more than 99% is singly ionized. Through recombinations, this Mg II reservoir eventually refills the levels at $\chi_{exc} \sim 7$ eV through a collisionally coupled ladder of Rydberg states of Mg I. The emission of the 12 μm lines originates from levels next above the states of the optically thin $\chi_{exc} \sim 7$ eV lines. It should be noted that there is a strong collisional coupling between Rydberg states with $\Delta n = 1$, which ensures that the replenishment proceeds stepwise down through the Rydberg states (Rutten & Carlsson 1994).

Avrett et al. (1994) find that the solar 12 μm emission is sensitive to collision and photoionization rates but quite insensitive to the atmospheric parameters. The atmospheric parameters we use for Procyon are quite well determined (see § 3). In the following sections, we investigate our modeling by discussing the ionizing radiation field, the assumption of homogeneity, the atomic model, and the collisional data.

[5] Where *l* is the azimuthal quantum number.

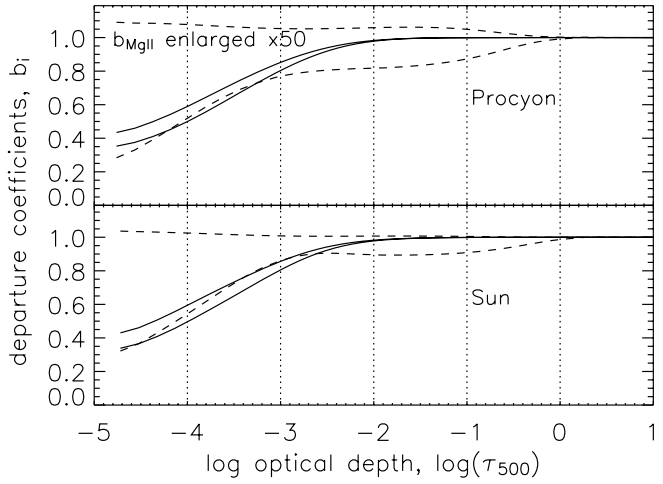

FIG. 5.—Departure coefficients as a function of optical depth at 500 nm ($\log \tau_{500}$) for the levels involved in the 811.6 and 818.1 cm^{-1} lines (*solid lines*). The upper panel shows our calculations for Procyon, and the lower panel shows the values for the Sun. The upper levels of the two Mg I lines behave in the same way, as do the lower levels. However, the lower levels depart more from LTE. The upper dashed lines show the departure coefficient of the Mg II ground state, showing a larger magnitude for the Sun. The lower dashed lines show the ground state of Mg I.

4.1. *The Ionizing UV Field*

The treatment of the ionizing UV field is of great importance since, in general, the main non-LTE effect in magnesium is caused by the photoionization, and it affects the strengths of the Mg I lines at 12 μm (Bruls et al. 1995). The UV field influences the ionization stage of magnesium, and, more important, the photoionization from low-lying levels closes the non-LTE flow and populates the Rydberg levels. The ionization state is determined mainly by the photoionization and radiative recombination equilibria of the three lowest levels: $3s3s^1S^e$ (with an ionization edge at 1621 Å), $3s3p^3P^o$ (2513 Å), and $3s3p^1P^o$ (3756 Å). The radiative cross sections to and from these levels are well determined (see, e.g., Carlsson et al. 1992b or Figs. 6*a* and 6*b*).

To investigate the sensitivity of the 12 μm emission lines to the UV field, we simulate a change in the UV field by artificially manipulating the photoionization cross section from these three lowest states. This can be justified because the photoionization rate per unit volume is an integral of the product of the cross section and the mean intensity (i.e., UV field for the three lowest cross sections) and is given by

$$\text{rate} = 4\pi \int_{\nu_0}^{\infty} \frac{\sigma(\nu) J_\nu}{h\nu}\, d\nu, \qquad (1)$$

with $\sigma(\nu)$ being the monochromatic cross section per particle, J_ν the mean intensity, and ν_0 the threshold frequency. For the ground state $3s3s^1S^e$ with an ionization edge at 1621 Å, a change by as much as a factor of 10 does not affect the emergent intensity at 12 μm at all. Therefore, the calculated flux and the modeled photoionization cross section at that ionization edge were not important for the ionization balance. This behavior is likely to be a result of the fact that the stellar flux at this edge is so low that it does not affect the ionization balance. Changing the cross sections for the other two low-lying

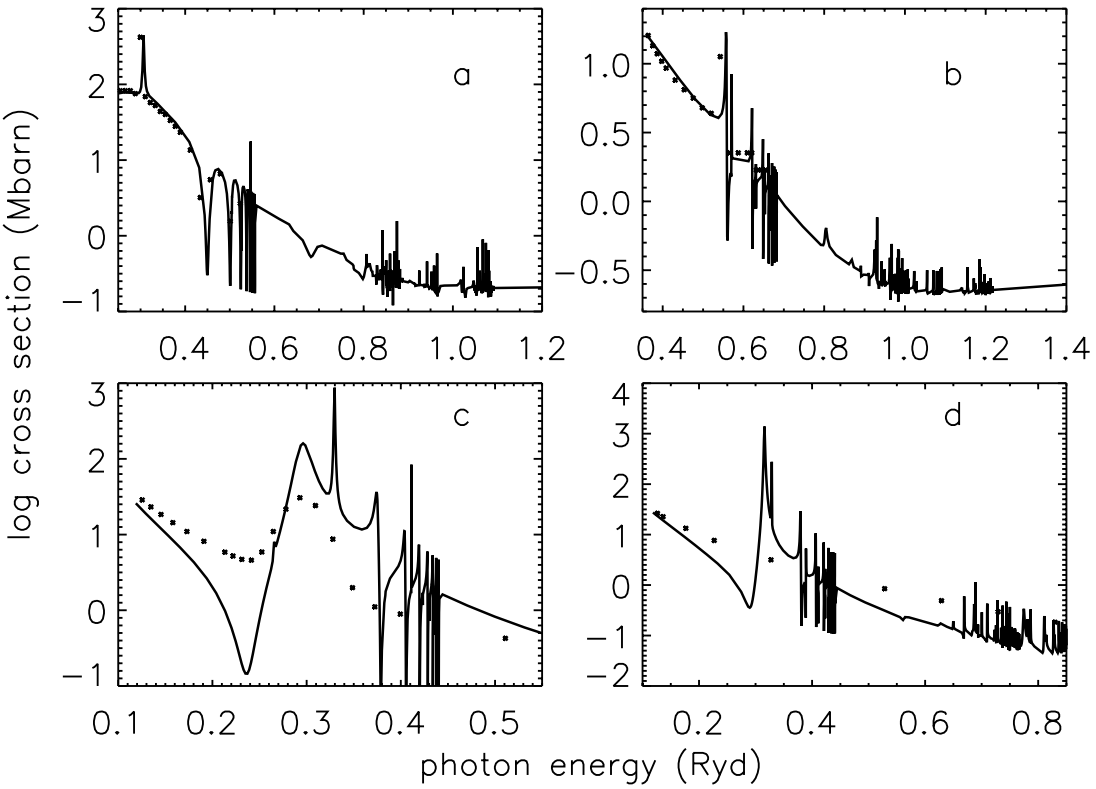

FIG. 6.—Photoionization cross sections from the Carlsson et al. (1992b) atom (*dots*) and from the OP (Butler et al. 1993; *solid lines*). The four panels show the four most influential transitions, in order of decreasing importance: (*a*) ionization from $3s3p^1P^o$, (*b*) $3s3p^3P^o \rightarrow$ Mg II, (*c*) $3s3d^3D^e \rightarrow$ Mg II, and (*d*) $3s4p^3P^o \rightarrow$ Mg II.

levels by 25% changes the strengths of the emission lines by less than 10% and 25%, respectively.

One way of testing the ionizing flux is to compare the modeled, emergent UV flux with satellite measurements. This will not ensure that the calculated flux is correct at all depths, especially at depths at which the ionization takes place, but it will give an indication of how appropriate the modeled fluxes are. The most important fluxes are the ones at the ionization edges, partly because the bound-free cross section decreases rapidly away from the edge and partly because of the fact that the ionizing mean intensity field decreases rapidly in the Wien limit of the star's spectral energy distribution; the measured flux at 1621 Å is, e.g., a factor of 50 times lower than the flux at 2513 Å. Thus, we are most interested in testing the fluxes around 2513 and 3756 Å.

The *International Ultraviolet Explorer* (*IUE*)[6] recorded UV spectra for a large number of stars, including Procyon. The SWP spectrometer covered the 1150–1980 Å range, and the LWR spectrometer covered the 1850–3350 Å region. Correcting for the distance to Procyon and assuming the above-mentioned radius of the star, it is possible to compare our modeled spectrum in the UV with the low-resolution *IUE* spectrum of Procyon. This is shown in Figure 7, where the fluxes are given on a logarithmic scale. The modeled flux is the low-resolution OS spectrum generated directly from the MARCS code. The *IUE* data files, retrieved from the *IUE* Newly Extracted Spectra (INES) database, are SWP43428 and LWR09108. The oval aperture ($10'' \times 20''$) of the telescope onboard the satellite ensures that all flux from the star is recorded. We find that the emergent flux (F_λ) from the model is in fair agreement with the observations. At longer wavelengths, including the interesting edge at 2513 Å, the agreement is very good, with differences within 25%; see Figure 7. As the flux increases at longer wavelengths, the agreement can be expected to be even better (e.g., for the ionization edge at 3756 Å). For the wavelength range 1800–2400 Å, the modeled fluxes are within a factor of 2, and for shorter wavelengths there are larger discrepancies.

We therefore conclude that our modeled fluxes can be used with some confidence. The difference between the observed *IUE* flux and the modeled flux, of importance for the edges at

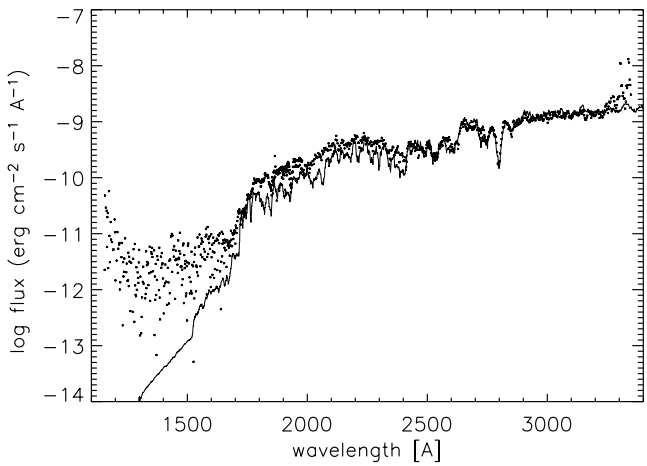

FIG. 7.—UV flux measured by the *IUE* (*dots*). The solid line shows the flux we model with the MARCS model atmosphere code, taking into account a distance to Procyon of 3.5 pc (calculated from a *Hipparcos* parallax of 286 mas) and the assumed radius of 2.1 $R_\odot$.

[6] Based on INES data from the *IUE*.

2513 Å and close to 3756 Å, is not large enough to affect the modeled 12 μm fluxes appreciably.

4.2. *Atmospheric Homogeneity*

The granulation pattern in Procyon is shallower than that for the Sun. According to the simulations of Allende Prieto et al. (2002), the layers in Procyon showing maximum temperature contrast caused by convection lie where the optical continuum is formed, $0 < \log \tau_{500} < 0.5$ ("naked granulation"). For the Sun the corresponding layers lie beneath the continuum-forming layers ($\log \tau_{500} \sim 1$). The solar emission lines are not expected to be affected much by asymmetries caused by granules (Rutten & Carlsson 1994). The continuum is formed so much farther out in the solar photosphere that the line formation is not greatly affected by the inhomogeneities. Therefore, a plane-parallel, homogeneous model photosphere is able to reproduce the solar emission lines well. The Mg I emission lines in Procyon have contribution functions extending over depths of approximately $-4 < \log \tau_{500} < -1$ but could be affected.

A more realistic treatment of the convection in the atmosphere would have been preferred but requires atmospheric models including three-dimensional hydrodynamic modeling of the convection (Asplund et al. 2000; Allende Prieto et al. 2002). These sorts of models are not yet readily available. An assessment of the uncertainties introduced by using traditional models, which describe convection by the mixing-length approximation, is given by Allende Prieto et al. (2002). They studied Procyon and scrutinized the differences in using traditional and hydrodynamic models. For example, the difference in the abundance of iron is found to be less than 0.05 dex.

4.3. *The Radiative Part of the Atomic Model*

The atomic model data consist of energy levels, statistical weights, oscillator strengths ($f_{\rm osc}$), broadening parameters (for natural, van der Waals, and Stark broadening), and photoionization rates. Furthermore, collisional data for line transitions and collisional ionization are included. The data used in our calculation are described in Carlsson et al. (1992b). We find that the sensitivity of the model emission lines to the atomic data in the model atom are of the same kind and order as that found in Carlsson et al. (1992b); i.e., a factor of 2 change in any of the radiative rates results in a change of the emission by less than 10%, except for the transition itself. The collisional rates are less influential.

After our model was set up by Carlsson et al. (1992b), newer data appeared in the literature, especially concerning bound-bound and bound-free radiative transitions, i.e., $f_{\rm osc}$-values, photoionization cross sections, and broadening parameters. Therefore, we have compared our data for the most important transitions affecting the Mg I emission lines with the data available at present from the Opacity Project (OP; Butler et al. 1993).

The OP data include only levels and transitions for Mg I states with quantum numbers $n < 9$ and $l < 5$. Zhao et al. (1998) and Przybilla et al. (2001) write that the transition probabilities from the OP data are accurate to within $\pm 10\%$. We find that our $gf_{\rm osc}$-values are in agreement with the OP data to within 10% and for most cases to within 5%. For the 12 μm transitions, our $gf_{\rm osc}$-values differ from those used by Zhao et al. (1998) by approximately 50%–60%. While our $gf_{\rm osc}$-values come from Carlsson et al. (1992b) and are calculated based on Green et al. (1957), the $gf_{\rm osc}$-values used by Zhao et al. (1998) are calculated based on Bates & Damgaard (1949). Note that the $f_{\rm osc}$-values enter into the calculations of the collisional rates, thus affecting them by the same amount.

In the Carlsson et al. (1992b) atom, the photoionization cross sections are given in a smoothed fashion with some of the most important fine structures, such as resonances, taken into account. In Figure 6 we show the most recent OP data for the photoionization cross sections for the most important transitions affecting the 12 μm emission lines. Przybilla et al. (2001) assume the uncertainty in the OP photoionization data to be of the order of $\pm 10\%$. The two most influential cross sections are in good agreement with the OP data. The other two differ more, especially at higher photon energies, i.e., the farther away one gets from the ionization edge. As these ionization channels close the non-LTE flow, they could be of importance for the strengths of the emission lines. Therefore, we repeated our non-LTE calculation using the OP data instead of the smoothed cross sections used in the Carlsson et al. (1992b) atom for these transitions. We find this hardly affects the emission at all.

New data on Stark broadening due to impacts of charged particles on Mg I have been published by Dimitrijević & Sahal-Bréchot (1996). Rydberg atoms are physically large, and quadratic Stark broadening of Rydberg transitions can be important (see, e.g., Carlsson et al. 1992b). Dimitrijević & Sahal-Bréchot (1996) show that the Carlsson et al. (1992b) choice of Stark broadening is a factor of 2.5 too low compared to new calculations. Recalculating our model of the Mg I lines with the appropriate Stark broadening factor, we find little change.

To summarize, we are confident that the radiative parameters of the Mg I atom presented by Carlsson et al. (1992b), which we use, are up-to-date and perform well for the Mg I emission lines.

4.4. *Collisional Data*

In the model atom provided by Carlsson et al. (1992b), transitions caused by collisions with electrons are incorporated mostly using the impact-parameter approximation of Seaton (1962). This provides a consistent set of collisional rates accurate to within a factor of 2 (Carlsson et al. 1992b). Rates from the ground state to a few of the lowest states are taken from Mauas et al. (1988). As discussed by Carlsson et al. (1992b) and Bruls et al. (1995), the most important aspect of the collisional data is their homogeneity throughout the atom. The internal consistency is significant for the setup of the non-LTE populations throughout the atom and, therefore, for the formation of the 12 μm lines.

From our non-LTE calculation we see that the collisional rates are larger than the radiative rates for the levels involved in the generation of the emission lines by a factor of 3 at the line center and a factor of 50 at the extremes of the line wings. The fact that collisions dominate the Rydberg transitions was also found for the solar case by Carlsson et al. (1992a). The collisions play an important role in setting up the Rydberg ladder through which the recombined atoms de-excite. In order to reproduce the fits of the solar lines, we have increased the collisional cross sections for the two 12 μm lines by 50% compared to the ones given by the impact approximation, which is well within the uncertainties. Finally, we also find that changing the collisional ionization by as much as a factor of 10 did not result in any noticeable difference.

The Zhao et al. (1998) non-LTE model includes inelastic, allowed neutral-hydrogen collisions, which should be increasingly important for cool, metal-poor stars. The strength and energy dependence of these collisions were empirically

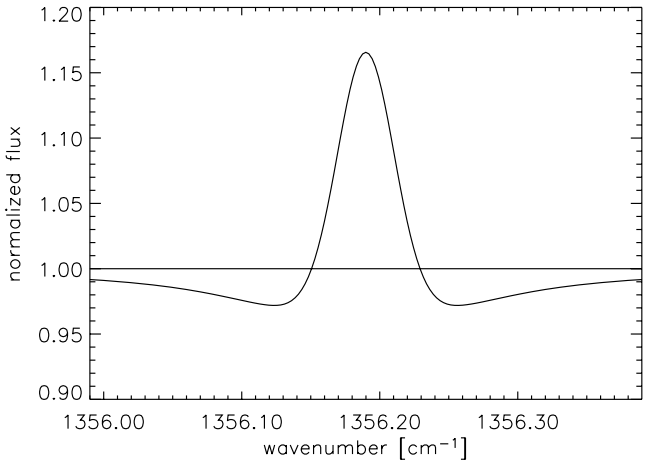

FIG. 8.—Prediction of the strong Mg I emission line at 1356.2 cm^{-1}. It is plotted on the same relative scale as in Figs. 1 and 2, making a direct comparison possible. The troughs in the flux spectrum of this line are pronounced and should be detectable at a signal-to-noise ratio similar to that of our present observations of the other two Mg I lines.

determined. The authors show that including the collisions influences the line cores of optical and NIR Mg I lines by reducing the non-LTE effects by approximately 50% and results in better fits to the solar Mg I lines they considered. The line cores are formed at shallow depths in the atmosphere where electron collisions are less important and hydrogen collisions can be expected to be important. Zhao et al. (1998) incorporate the collision rates with the Drawin (1969) formula. These rates are, however, subsequently scaled with a factor that decreases exponentially with the excitation energy of the upper level involved in the collision, thus not affecting the 12 μm Mg I emission lines. We chose not to include these extra collisions, since their global effect on the departure coefficients of the Mg I atom is assumed to be small. The hydrogen collisions can, however, have an effect on the magnesium abundance inferred from optical lines, which usually enters the analysis of the Mg I IR emission lines as an additional unknown. However, as mentioned above, in our analysis of Procyon we have assumed solar composition.

4.5. *Further Observations*

With our model we find that a stronger line is at 1356.19 cm^{-1}, generated by the $6h^{1,3}H^o \rightarrow 5g^{1,3}G^e$ transition of neutral magnesium. The model prediction for Procyon is shown in Figure 8. The troughs are more pronounced than those of the 811.6 and 818.1 cm^{-1} lines and should be detectable. They are of interest because they map the minimum of the source function as a function of depth in the atmosphere. The troughs are very broad, of the order of $\sim$75 km s^{-1}, and will require care when normalizing the spectra to preserve the troughs during data reduction. Ground-based observations of this line require very low column density of telluric water vapor, but future observations from the Stratospheric Observatory for Infrared Astronomy (SOFIA) will be fairly routine. Because molecular transitions of H_2O, SiO, and CO are common throughout this region, we expect the 1356.19 cm^{-1} line to be best for stars hotter than spectral type M.

5. DISCUSSION AND CONCLUSIONS

The splitting of the solar 12 μm lines in magnetically active surface regions shows normal Zeeman triplet splitting with one π and a pair of σ components, although all the components actually have tightly grouped substructure. The π and σ components are separated by a width given by an effective Landé factor of approximately 1, which was experimentally found by Lemoine et al. (1988). The average separation between the two σ components is given by

$$\Delta\lambda_B = 2 \times 4.67 \times 10^{-9} g \lambda_0^2 B \ \mu\text{m}, \quad (2)$$

where g is the Landé factor, λ_0 is the unperturbed wavelength of the line in microns, and B is the magnetic field strength in gauss. The strength of the solar magnetic fields puts the Zeeman effect in the Paschen-Back regime for these lines (Bruls et al. 1995).

There are advantages to Zeeman magnetic field studies using infrared lines compared to optical ones. In addition to less line blending due to the lower line density (see, e.g., Ryde et al. 2004), infrared spectral lines have larger Zeeman sensitivity. Optical lines most often do not show large enough Zeeman separation to be disentangled from other broadening mechanisms of the line. The ratio of the separation of the Zeeman splitting ($\Delta\lambda_B \sim g\lambda^2 B$) and the nonmagnetic Doppler width ($\Delta\lambda_D \sim \lambda$) is given by $\Delta\lambda_B/\Delta\lambda_D \sim g\lambda B$. Thus, the ratio grows with wavelength and, consequently, it is easier to detect Zeeman-split lines in the infrared. With larger Zeeman separation between the components, the analysis is simpler.

Although the largest Landé factors for optical and NIR transitions are roughly 3, while the Mg I lines at 12 μm have an effective Landé factor of 1, moving to 12 μm from the optical and NIR increases the sensitivity by at least a factor of 8 and 3, respectively. According to Solanki (1994), it should be possible to measure solar magnetic field strengths as low as 150–200 G from line splitting, and fields down to 100 G are measurable through (very) careful profile fits. (A large magnetic field would split the line, and, in the case of low field strength, it would act as an additional broadening.) Bruls et al. (1995) discuss measurements of the Stokes parameters of the solar 12 μm lines affected by solar magnetic fields and indicate that field strengths of approximately 200 G are measurable through Stokes V line splitting. They also show that line splitting in the Stokes I light is reliable only for strengths greater than 500 G.

It should be noted that, especially for the broadened lines, the sensitivity for detecting magnetic fields for a disk-averaged stellar Mg I spectrum will also depend on the filling factor (f) of the field over a stellar surface (see, e.g., Valenti et al. 1995). In the simplest case, a stellar magnetic field can be modeled by a two-component model, with one magnetic component with a constant field strength, B, over a fraction, f, of the surface and one nonmagnetic component, the latter covering $(1 - f)$ of the stellar surface (Solanki 1992). Furthermore, in a field-free approximation (see, e.g., Bruls et al. 1995) one can assume that a magnetic field does not affect the departure coefficients significantly. The non-LTE calculations can, therefore, be made for a nonmagnetic environment (N. E. Piskunov 2004, private communication).

We have not resolved any magnetic components on Procyon and see only single-peaked features that are well fitted by Gaussian distributions. Given the absence of any resolved σ components, we can estimate the field strength and filling factor that would have produced detectable, separate σ components. We consider the line at 811.578 cm^{-1} because the signal-to-noise ratio for this line, 130:1, is higher than that for

the 818.058 cm^{-1} line. Our estimate considers only the magnetic field strength and filling factor at the photospheric height that dominates the line formation. Pressure equilibrium and magnetic flux conservation suggest that magnetic flux tubes will have a larger filling factor and weaker field strength higher in the photosphere where the gas pressure is lower.

Given our observations, we believe we would have detected resolved σ components if the magnetic field strength had been $B > 830$ G and the filling factor $f > 26\%$. In this simplistic estimate, we assume the observed line, which has a peak height of 0.135 above the normalized continuum, comes from the nonmagnetic region with filling factor $(1 - f)$. Given the signal-to-noise ratio, a 3 σ detection would require a peak value of 0.024 above the normalized continuum. If the efficiency for producing the two σ components in the magnetic region is the same as that for producing the central peak from the nonmagnetic region, we can calculate that the magnetic filling factor must be approximately 26%. To determine the maximum field strength allowed by our observations, we consider a separation between the two σ components of 28.5 km s^{-1} (3 times the FWHM of the detected line) to be sufficiently resolved that we would resolve the separate peaks. Using equation (2), such a splitting would require a magnetic field strength of 830 G. For comparison, it can be noted that fields similar to and stronger than this have been detected for other stars. For example, Johns-Krull et al. (1999) measure a surface-averaged mean field from IR observations of the T Tauri star BP Tau of $\Sigma Bf = 2.6 \pm 0.3$ kG, and Valenti et al. (1995) find that 9% of the deep photosphere of the active star ϵ Eri is filled with a 1.4 kG field.

A further diagnostic value of the 12 μm lines is their different height of formation compared with lines at, e.g., 1.5 μm. The 1.5 μm lines are commonly used in solar magnetic field observations and sample the opacity minimum. For the Sun, the lateral expansion of magnetic flux tubes with height dilutes the field strength (Deming et al. 1988). Thus, fields measured at 12 μm, sampling higher regions, may be lower than those measured by lines lying at 1.5 μm. Because of the different depth dependence, comparisons of Zeeman splitting from lines at different frequencies can start to trace the vertical structure of magnetic flux tubes (Bruls et al. 1995).

While the 12 μm lines provide high sensitivity to magnetic fields, observing these lines is still difficult. As 8–10 m telescopes become equipped with high-resolution, mid-infrared spectrographs, many more stars will prove suitable targets. We are confident that high-resolution observations of the 12 μm lines will be an important tool for measuring stellar magnetic fields in the future. We have shown that we understand the formation of the 12 μm lines, not only for the Sun but also for Procyon, and that the non-LTE calculation, based on the one for the Sun, is still up-to-date.

We would like to thank Mats Carlsson for providing the Mg I model atom used in this study. We gratefully acknowledge our fruitful discussions with Kjell Eriksson and Bengt Gustafsson, and we thank Karin Ryde for linguistic aid. We are grateful for the help of John Lacy and Thomas Greathouse of the TEXES team, as well as the IRTF staff. This work was supported in part by the Swedish Research Council, the Swedish Foundation for International Cooperation in Research and Higher Education, and Stiftelsen Blanceflor Boncompagni-Ludovisi, née Bildt. The construction of TEXES was supported by grants from the NSF, and observing with TEXES was supported by the Texas Advanced Research Program. A. J. Korn was supported by the Leopoldina Foundation/Germany under grant BMBF-LPD 9901/8-87.

REFERENCES

Allende Prieto, C., Asplund, M., López, R. J. G., & Lambert, D. L. 2002, ApJ, 567, 544
Asplund, M., Nordlund, Å., Trampedach, R., Allende Prieto, C., & Stein, R. F. 2000, A&A, 359, 729
Avrett, E. H., Chang, E. S., & Loeser, R. 1994, in IAU Symp. 154, Infrared Solar Physics, ed. D. M. Rabin, J. T. Jefferies, & C. Lindsey (Dordrecht: Kluwer), 323
Bates, D. R., & Damgaard, A. 1949, Philos. Trans. R. Soc. London A, 242, 101
Brault, J., & Noyes, R. 1983, ApJ, 269, L61
Bruls, J. H. M. J., & Solanki, S. K. 1995, A&A, 293, 240
Bruls, J. H. M. J., Solanki, S. K., Rutten, R. J., & Carlsson, M. 1995, A&A, 293, 225
Butler, K., Mendoza, C., & Zeippen, C. J. 1993, J. Phys. B, 26, 4409
Carlsson, M. 1986, A Computer Program for Solving Multi-Level Non-LTE Radiative Transfer Problems in Moving or Static Atmospheres (Rept. No. 33; Uppsala: Uppsala Astronomical Obs.)
Carlsson, M., Rutten, R. J., & Shchukina, N. G. 1990, in Proc. 6th European Meeting on Solar Physics: The Dynamic Sun, ed. L. Dezso (Debrecen: Hungarian Acad. Sci.), 260
———. 1992a, in ASP Conf. Ser. 26, Cool Stars, Stellar Systems, and the Sun, ed. M. S. Giampapa & J. A. Bookbinder (San Francisco: ASP), 518
———. 1992b, A&A, 253, 567
Chang, E. S., Avrett, E. H., Noyes, R. W., Loeser, R., & Mauas, P. J. 1991, ApJ, 379, L79
Chang, E. S., & Noyes, R. W. 1983, ApJ, 275, L11
Deming, D., Boyle, R. J., Jennings, D. E., & Wiedemann, G. 1988, ApJ, 333, 978
Dimitrijević, M. S., & Sahal-Bréchot, S. 1996, A&AS, 117, 127
Drawin, H. W. 1969, Z. Phys., 225, 470
Fuhrmann, K. 1998, A&A, 338, 161
Gray, D. F. 1981, ApJ, 251, 152
Green, L. C., Rush, P. P., & Chandler, C. D. 1957, ApJS, 3, 37
Grevesse, N., & Sauval, A. J. 1998, Space Sci. Rev., 85, 161
Gustafsson, B., Bell, R. A., Eriksson, K., & Nordlund, A. 1975, A&A, 42, 407
Johns-Krull, C. M., Valenti, J. A., & Koresko, C. 1999, ApJ, 516, 900
Korn, A. J. 2002, Ph.D. thesis, Univ. Munich
Lacy, J. H., Richter, M. J., Greathouse, T. K., Jaffe, D. T., & Zhu, Q. 2002, PASP, 114, 153
Lemke, M., & Holweger, H. 1987, A&A, 173, 375
Lemoine, B., Demuynck, C., & Destombes, J. L. 1988, A&A, 191, L4
Mauas, P. J., Avrett, E. H., & Loeser, R. 1988, ApJ, 330, 1008
Muglach, K., & Solanki, S. K. 1992, A&A, 263, 301
Murcray, F. J., Goldman, A., Murcray, F. H., Bradford, C. M., Murcray, D. G., Coffey, M. T., & Mankin, W. G. 1981, ApJ, 247, L97
Piskunov, N. E., Kupka, F., Ryabchikova, T. A., Weiss, W. W., & Jeffery, C. S. 1995, A&AS, 112, 525
Przybilla, N., Butler, K., Becker, S. R., & Kudritzki, R. P. 2001, A&A, 369, 1009
Rutten, R. J., & Carlsson, M. 1994, in IAU Symp. 154, Infrared Solar Physics, ed. D. M. Rabin, J. T. Jefferies, & C. Lindsey (Dordrecht: Kluwer), 309
Ryde, N., Gustafsson, B., Eriksson, K., & Wahlin, R. 2004, in Proc. ESO Workshop on High Resolution Infrared Spectroscopy in Astronomy, ed. H. U. Kaeufl, A. Moorwood, & R. Siebenmorgen (Berlin: Springer), in press
Ryde, N., & Richter, M. J. 2004, ApJ, 611, L41
Saar, S. H. 1988, ApJ, 324, 441
Seaton, M. J. 1962, Proc. Phys. Soc., 79(6), 1105
Solanki, S. 1992, in ASP Conf. Ser. 26, Cool Stars, Stellar Systems, and the Sun, ed. M. S. Giampapa & J. A. Bookbinder (San Francisco: ASP), 211
Solanki, S. K. 1994, in IAU Symp. 154, Infrared Solar Physics, ed. D. M. Rabin, J. T. Jefferies, & C. Lindsey (Dordrecht: Kluwer), 393
Solanki, S. K., Rueedi, I. K., & Livingston, W. 1992, A&A, 263, 312
Uitenbroek, H., & Noyes, R. W. 1996, in ASP Conf. Ser. 109, Cool Stars, Stellar Systems, and the Sun, ed. R. Pallavicini & A. K. Dupree (San Francisco: ASP), 723
Valenti, J. A., Marcy, G. W., & Basri, G. 1995, ApJ, 439, 939
Zhao, G., Butler, K., & Gehren, T. 1998, A&A, 333, 219